Korean J. Chem. Eng., 33(1), 33-45 (2016)
DOI: 10.1007/s11814-015-0124-9

pISSN: 0256-1115
eISSN: 1975-7220

Estimation of local concentration from measurements of stochastic adsorption dynamics using carbon nanotube-based sensors

Hong Jang*, Jay H. Lee*,†, and Richard D. Braatz**

*Department of Biomolecular and Chemical Engineering, Korea Advanced Institute of Science and Technology (KAIST), 291, Daehak-ro, Yuseong-gu, Daejeon 34141, Korea
**Department of Chemical Engineering, Massachusetts Institute of Technology (MIT), 77 Massachusetts Ave, Cambridge, MA 02139, United States of America
(*Received 16 February 2015 • accepted 8 June 2015*)

Abstract−This paper proposes a maximum likelihood estimation (MLE) method for estimating time varying local concentration of the target molecule proximate to the sensor from the time profile of monomolecular adsorption and desorption on the surface of the sensor at nanoscale. Recently, several carbon nanotube sensors have been developed that can selectively detect target molecules at a trace concentration level. These sensors use light intensity changes mediated by adsorption or desorption phenomena on their surfaces. The molecular events occurring at trace concentration levels are inherently stochastic, posing a challenge for optimal estimation. The stochastic behavior is modeled by the chemical master equation (CME), composed of a set of ordinary differential equations describing the time evolution of probabilities for the possible adsorption states. Given the significant stochastic nature of the underlying phenomena, rigorous stochastic estimation based on the CME should lead to an improved accuracy over than deterministic estimation formulated based on the continuum model. Motivated by this expectation, we formulate the MLE based on an analytical solution of the relevant CME, both for the constant and the time-varying local concentrations, with the objective of estimating the analyte concentration field in real time from the adsorption readings of the sensor array. The performances of the MLE and the deterministic least squares are compared using data generated by kinetic Monte Carlo (KMC) simulations of the stochastic process. Some future challenges are described for estimating and controlling the concentration field in a distributed domain using the sensor technology.

Keywords: Maximum Likelihood Estimation, Stochastic Processes, Chemical Master Equation, Carbon Nanotube-based Sensors, Sensor Array System

INTRODUCTION

Some of the most promising applications of nano-materials are in the sensors area [1,2]. Carbon nanotube (CNT)-based sensors have been developed and touted for having the ability to detect target molecules at a single molecule resolution [3]. A near-infrared fluorescent semiconducting single-walled carbon nanotube (SWNT), in particular, has been shown to induce stepwise fluctuations in the light intensity whenever an adsorption or desorption event of a target molecule occurs on its surface [4,5]. Several fluorescent SWNT sensors have been reported, with high selectivity for glucose [6], DNA [7], ATP [8], hydrogen peroxide [9,10], and nitric oxide [11, 12]. These sensors enable novel scientific investigations as well as open doors for engineering novel devices/processes. For example, with the nano-scale sensors for nitric oxide molecules, their roles in the body as signaling molecules can be investigated.

†To whom correspondence should be addressed.
E-mail: jayhlee@kaist.ac.kr
‡A preliminary version of this manuscript was published as H. Jang, J. H. Lee, and R. D. Braaz, Maximum-Likelihood Parameter Estimation for Detecting Local Concentration from a Carbon Nanotube-based Sensor, in the 10th International Symposium on Dynamics and Control of Process Systems, Mumbai, India.

An important challenge occurs at the sensor level in translating changes in the light intensity, which can be translated into the number of adsorbed molecules on the surface of the sensor, to variations in the local concentration of a target molecule surrounding the sensor. This task is complicated by the fact that the adsorption/desorption phenomena occurring at the nanoscale are highly stochastic. For a reliable estimation of local concentration at that length scale, use of a stochastic model describing the evolution of the probability distribution among all possible states may be needed. As an estimation problem, the translation of the adsorption data on the sensor surface into local concentration estimates surrounding the sensor is the main topic addressed by this article.

Stochastic dynamics with continuous states can be modeled by Langevin dynamics or the Fokker-Planck equation. However, many nano-scale systems involve discrete states, and their stochastic dynamics can be conveniently modeled by the chemical master equation (CME) [13]:

$$\frac{dP(\sigma, t)}{dt} = \sum_{\sigma'} W(\sigma', \sigma)P(\sigma', t) - \sum_{\sigma'} W(\sigma, \sigma')P(\sigma, t) \quad (1)$$

where $P(\sigma, t)$ is the probability of the system being in state σ at time t, and $W(\sigma', \sigma)$ is the transition rate from state σ' to state σ. The CME describes the time evolution of the probability distribution among all possible configurations. The CME (1) can be written as

$$\frac{d\mathbf{x}(t)}{dt} = \mathbf{A}(t;\theta)\mathbf{x}(t) \quad (2)$$

where $\mathbf{x}(t)$ is the single state vector containing all the probability variables and $\mathbf{A}(t;\theta)$ is the matrix collecting all transition rates, which have dependence on the parameter vector θ containing parameters related with phenomena at the molecular scale, such as chemical reactions, adsorption/desorption, and diffusion. In the specific system, θ contains an adsorption rate constant, which is proportional to the local concentration of target molecules surrounding the sensor. The common approach for solving the chemical master equation is to perform kinetic Monte Carlo (KMC) simulations to obtain approximate solutions. However, the KMC approach typically demands a very large number of simulations to be performed for a close approximation of the exact solution, and is not suitable for use in real-time estimation.

An analytical solution was derived for the CME for a monomolecular reaction system by Jahnke and Huisinga [14]. Their analysis modeled the monomolecular adsorption and desorption process as a birth-and-death process, which led to a Poisson or a multinomial distribution of the population for an open or a closed system, respectively. The analytical form of the solution makes possible an efficient estimation of parameters appearing in the CME. Based on this idea, maximum likelihood estimation (MLE) of the adsorption rate constant for the SWNT sensor system has been proposed [15-17].

On the other hand, the benefit from adopting a more complex stochastic estimation method over conventional deterministic methods like least squares in this context has not been assessed fully. In addition, the previous works treated only constant local concentration for an isolated single sensor, which is not realistic for a sensor system working in a real environment. This article, in addition to considering constant local concentration, examines time-varying concentration, which needs to be followed by the SWNT sensor array system. This work provides a basis to build a state estimator that recursively estimates the distributions of certain target molecules over a spatial regime. For this, we employed mass transport phenomena such as diffusion into the state of target molecules and apply it to distributed nano-sensors on 2D field.

We assessed the degree of performance improvement, realized by adopting the rigorous stochastic estimation approach of MLE in place of the conventional deterministic least-squares. The results indicate that more accurate estimation results can be obtained by adopting the estimation method that rigorously accounts for the stochastic nature. It is also shown that the simulations can be used to estimate the upper and lower detection limits of the analyte concentration for a given nano-sensor design, and to examine the effects of the parameter mismatch on estimation.

NANOSENSING SYSTEM

1. SWNT-based Sensor

As discussed by Cognet et al. [5], when molecules adsorb on the surface of the SWNT-based sensor, the fluorescence gets partially quenched resulting in discretized light intensity decreases. Similarly, the light intensity increases when molecules desorb from the surface. Fig. 1 illustrates the basic SWNT sensing mechanism. The SWNT surface functionalization (e.g., wrapping with DNAs) is to enhance selectivity and sensitivity for a specific chemical species (e.g., nitric oxide). A recently developed SWNT sensor provides a fluctuating light intensity time profile at the concentration range from 0.2 to 20 μM for nitric oxide molecules [11]. The detection range has a close relation with the sensing material design determining the frequency of adsorption and desorption events in the measurement data at the range, which can be interpreted as adsorption and desorption rates of the target molecule on the surface. In case of the SWNT sensor detecting nitric oxide molecules, dominant adsorption occurrence has been shown in the data due to a preferred design for high adsorption rate, while the SWNT sensor detecting hydrogen peroxide molecules has shown frequent adsorption and desorption occurrences in the data [9,11].

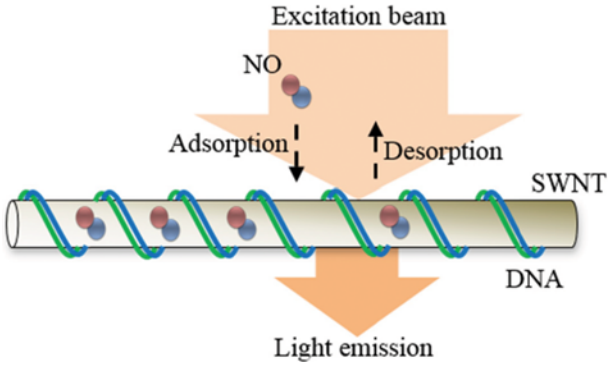

Fig. 1. A schematic of the SWNT-based sensing mechanism.

To specify the sensing system for modeling purposes, some assumptions should be made. The adsorption sites on the sensor surface are assumed to be evenly distributed as shown in Fig. 1.

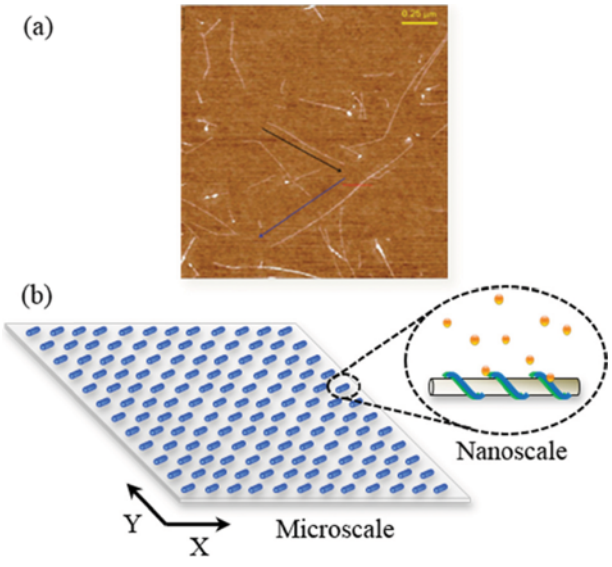

Fig. 2. (a) An atomic force microscopy (AFM) image of AT_{15}-SWNTs (Reprinted with permission from [27]. Copyright 2011 American Chemical Society) and (b) an ideal two-dimensional sensor array system.

The effect of diffusion of molecules on the SWNT surface can be ignored since the stepwise change of light intensity only occurs from adsorption and desorption events, not molecule movements [5]. By counting the number of step changes in the intensity, the number of adsorption and desorption events and thus the total number of adsorbed molecules can be deduced. For a typical SWNT sensor having a mean nanotube length of 10 μm, the maximum number of the adsorption sites is about 10 [11].

Synthesized SWNT-based sensors can be placed in a two-dimensional sensor array covering an area of up to ten or more squared centimeters [11]. For example, Fig. 2 shows the SWNT sensor array composed of single-stranded $d(AT)_{15}$ DNA oligonucleotide wrapped SWNTs (AT_{15}-SWNTs) detecting nitric oxide molecules selectively. An individual suspension of AT_{15}-SWNTs in the array can be detected by atomic force microscopy (AFM, Fig. 2(a)) and its ideal system can be depicted as an evenly distributed sensor array on a two-dimensional field (Fig. 2(b)). From this array system, the objective is to estimate time profiles of two-dimensional concentration fields of target molecules. This spatiotemporal profile information can be useful for monitoring and control of a two-dimensional (2D) spatial system (e.g., see [18] and citations therein).

2. Adsorption Model

In developing a kinetic model for the SWNT sensor [16], free target molecules, A, in a surrounding liquid are assumed to adsorb onto available sites of the nanotube segment, θ, to form bound molecules, $A\theta$, through the reversible adsorption reaction:

$$A + \theta \underset{k_D}{\overset{k'_A}{\rightleftharpoons}} A\theta \tag{3}$$

where k'_A [s^{-1}] and k_D [s^{-1}] are adsorption and desorption rate constants, respectively. The adsorption rate is generally considered to be a pseudo-first-order in the concentration of target molecules proximate to the sensor and the number of unoccupied sites, and the desorption rate is assumed to be a pseudo-first-order in the number of occupied sites [16], so the associated rates are expressed as

$$r_A = k'_A N_\theta \tag{4}$$

$$r_D = k_D N_{A\theta} \tag{5}$$

$$k'_A = k_A C \tag{6}$$

where N_θ is the number of empty sites, $N_{A\theta}$ is the number of occupied sites, k_A is a constant factor in the adsorption coefficient, and C is the local concentration of the surrounding target molecules. The local concentration of target molecules in the liquid phase is sufficiently high (~μM) such that it is not affected by the adsorption and desorption events (maximum 10 molecules on the sensor).

For each local sensor, a CME can be formulated that is composed of differential equations describing the evolution of the probabilities for all possible states of the system. For this system, the state can be defined as the number of adsorbed molecules, $N_{A\theta} \in [0, N_T]$, resulting in N_T+1 total possible states. Hence, it is assumed that exact locations of adsorbed molecules do not matter, just their total number. The probability of being in each state is denoted by, $P_i = \Pr(N_{A\theta}=i) \in [0, 1]$, where is the number of adsorbed molecules. The CME, along with the appropriate boundary equation, can be expressed by N_T+1 ordinary differential equations (ODEs):

$$\frac{dP_0(t)}{dt} = -P_0(t)[k'_A N_T] + P_1(t)[k_D] \tag{7}$$

$$\frac{dP_i(t)}{dt} = P_{i-1}(t)[k'_A(N_T-(i-1))] - P_i(t)[k_D i + k'_A(N_T-i)] + P_{i+1}(t)[k_D(i+1)], \ \forall i=1, 2, \ldots, N_T-1 \tag{8}$$

$$\frac{dP_{N_T}(t)}{dt} = P_{N_T-1}(t)[k'_A] - P_{N_T}(t)[k_D N_T] \tag{9}$$

subject to

$$\sum_{i=0}^{N_T} P_i(t) = 1 \tag{10}$$

$$0 \le P_i(t) \le 1, \ \forall i = 0, \ldots, N_T \tag{11}$$

On the other hand, the continuum (or average) model can be formed by writing just one differential equation for the number of adsorbed molecules (with the assumption that adsorption/desorption occur deterministically) from the rates (4) and (5):

$$\frac{d\tilde{N}_{A\theta}(t)}{dt} = r_A - r_D = k'_A(N_T - \tilde{N}_{A\theta}(t)) - k_D \tilde{N}_{A\theta}(t) \tag{12}$$

subject to

$$0 \le \tilde{N}_{A\theta}(t) \le N_T \tag{13}$$

The solution to the continuum Eq. (12) with constant concentration in (6) can be easily obtained for an arbitrary initial condition, $\tilde{N}_{A\theta}(0)$, as

$$\tilde{N}_{A\theta}(t) = \frac{N_T + (\tilde{N}_{A\theta}(0)(1+k_D/(k_A C)) - N_T)e^{-(k_A C + k_D)t}}{1 + k_D/(k_A C)} \tag{14}$$

where $\tilde{N}_{A\theta}(t)$ is the average value for the number of occupied sites at time .

In a real system, the adsorption rate constant, k'_A, can be time-varying due to variations in the concentration of surrounding molecules. For time-varying concentration in (6), the analytical solution

$$\tilde{N}_{A\theta}(t) = \frac{\int_0^t k_A C(r) N_T e^{\int_0^r (k_A C(s) + k_D) ds} dr + \tilde{N}_{A\theta}(0)}{e^{\int_0^t (k_A C(u) + k_D) du}} \tag{15}$$

can be obtained by applying the integrating factor. However, the general solution of (15) is fairly complex to evaluate, with an integral appearing within an integral. Even if C(t) has simple dynamics such as following an exponential decay function, the integrals within the solution may be difficult to evaluate analytically. For this reason, the solution (14) can be used by considering the previous measurement as an initial condition, $\tilde{N}_{A\theta}(t_{k-1})$, and assuming constant $C(t_{k-1})$ over each sampling time interval:

$$\tilde{N}_{A\theta}(t_k) = \frac{N_T + (\tilde{N}_{A\theta}(t_{k-1})(1+k_D/(k_A C(t_{k-1}))) - N_T)e^{-(k_A C(t_{k-1}) + k_D)\Delta t}}{1 + k_D/(k_A C(t_{k-1}))} \tag{16}$$

$$\Delta t = t_k - t_{k-1} \tag{17}$$

where k is the index for the time step and Δt is size of the time step

from the previous measurement. The solution at t_k depends on the solution at the previous time step of t_{k-1}, and Δt should be set sufficiently small for the approximation to be accurate.

BIRTH-AND-DEATH MARKOV PROCESS & ANALYTIC SOLUTION OF THE CME

Solving the CME numerically can become computationally expensive as the number of possible states grows. An analytical solution can be valuable in developing a real-time estimation approach that accounts fully for the stochastic nature of the molecular-level events. The birth-and-death model, which was studied by [14], provides a path to an analytic solution. The adsorption and desorption process can be considered as a birth-and-death process system [16]. Birth corresponds to a desorption event and death to an adsorption event.

For this system, the probability distribution follows a binomial distribution [14]. More specifically, this result says that the number of adsorbed molecules $N_{A\theta}$ at a time t_k is a random variable distributed as a binomial with the number of trials equal to N_T and probability parameter equal to $\lambda(t_k)$, which is related to $\tilde{N}_{A\theta}(t_k)$ calculated from the continuum Eq. (12) by

$$N_{A\theta}(t_k) \sim \mathcal{B}(N_T, \lambda(t_k)) \tag{18}$$

$$\Pr(N_{A\theta}(t_k)=i) = \binom{N_T}{i} (\lambda(t_k))^i (1-\lambda(t_k))^{N_T-i} \tag{19}$$

$$\lambda(t_k) = \frac{\tilde{N}_{A\theta}(t_k)}{N_T} \tag{20}$$

The adsorption rate constant (directly related to the local concentration of target molecule) is embedded in the expression for the probability parameter $\lambda(t_k)$.

With the assumption of the monomolecular adsorption reaction, the overall population can be divided into two subsets, representing occupied sites and unoccupied sites on the sensor. Then, with some arbitrary measured value of $N_{A\theta}$ at t_{k-1} (denoted hereafter by $\hat{N}_{A\theta}(t_{k-1})$), the distribution at the next time step can be derived as the convolution of two binomial distributions applicable to the "fully occupied" and "empty" subsets, which are of size $\hat{N}_{A\theta}(t_{k-1})$ and $1-\hat{N}_{A\theta}(t_{k-1})$, respectively. The first binomial distribution can be derived from (19) by assuming the sites are fully occupied initially. Similarly, the second binomial distribution can be derived from (19) by considering the initial state to be empty [14]:

$$N_{A\theta}(t_k) \sim B(\hat{N}_{A\theta}(t_{k-1}), \lambda^F(t_{k-1})) * B(N_T-\hat{N}_{A\theta}(t_{k-1}), \lambda^E(t_{k-1})) \tag{21}$$

$$\lambda^F(t_{k-1}) = \frac{1+k_D/(k_A C(t_{k-1}))e^{-(k_A C(t_{k-1})+k_D)\Delta t}}{1+k_D/(k_A C(t_{k-1}))} \tag{22}$$

$$\lambda^E(t_{k-1}) = \frac{1-e^{-(k_A C(t_{k-1})+k_D)\Delta t}}{1+k_D/(k_A C(t_{k-1}))} \tag{23}$$

If the expression for $\tilde{N}_{A\theta}(t_k)$ obtained by setting $\tilde{N}_{A\theta}(t_{k-1})=N_T$ in (16) is substituted into (20), the probability parameter $\lambda(t_{k-1})$ becomes equal to $\lambda^F(t_{k-1})$ in (22). The variable N_T cancels out and the expression is independent of it. If the same substitution is carried out by setting $\tilde{N}_{A\theta}(t_{k-1})=0$ in (16), $\lambda(t_{k-1})$ becomes $\lambda^E(t_{k-1})$ in (23). For a constant local concentration, $C(t_{k-1})$ in (22) and (23) is C for all time.

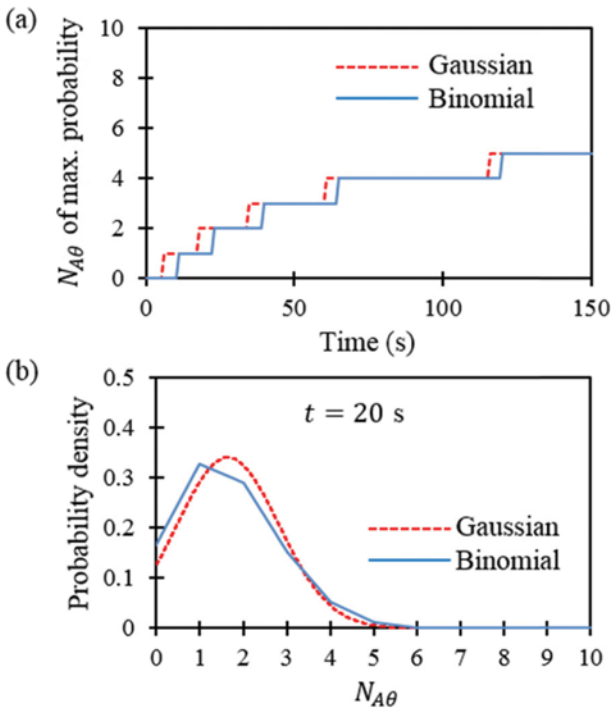

Fig. 3. Comparison of the binomial distribution and Gaussian distribution for k_A=1, k_D=10^{-2} and C=10^{-2}, and initially empty sites with (a) time profile of the number of adsorbed molecules with maximum probability and (b) distributions at t= 20 sec showing significant differences.

The adsorbed molecules on the sensor are now defined by a binomial random variable, which is not commonly studied in the estimation literature (most estimation methods assume Gaussian distributions, explicitly or implicitly). To show the difference explicitly, Fig. 3 compares the binomial distribution and the best approximating Gaussian distribution for the number of adsorbed molecules resulting from k_A=1, k_D=10^{-2} and C=10^{-2}, and initially empty sites. The number of adsorbed molecules corresponding to the maximum probability in the binomial distribution is not coincident with that in the Gaussian distribution (see Fig. 3(a)). In addition, the two distributions at t=300 seconds shown in the Fig. 3(b) differ significantly. It can be expected that estimation results based on the binomial distribution and Gaussian distribution would be different.

ESTIMATION METHOD FORMULATIONS

It is assumed that $k_A'(t)$ appearing in both the CME (7)-(9) and continuum Eq. (12) is proportional to the local concentration of target molecules, C(t), surrounding the sensor [16]. This assumption means that accurate estimation of $k_A'(t)$ translates directly into accurate estimation of the local concentration (with known adsorption parameter k_A), which is the desired system information. This article formulates and compares two representative estimation methods for the local concentration: (1) maximum likelihood estima-

tion (MLE) based on the probability distribution solution of the CME, and (2) least-squares estimation (LSE) based on the deterministic solution of the continuum equation.

1. Maximum Likelihood Estimation

For the MLE, the objective function is based on the joint probability distribution of the measurement sequence $\hat{\mathbf{N}}_{A\theta}(t_k)$ obtained for time steps k=1, …, N from sensors j=1, …, N_S in the system:

$$J_{MLE}(\mathbf{C}(t_k), k=0, \ldots, N-1) = \Pr(\hat{\mathbf{N}}_{A\theta}(t_N), \ldots, \hat{\mathbf{N}}_{A\theta}(t_1) | \mathbf{C}(t_{N-1}), \ldots, \mathbf{C}(t_0)) \quad (24)$$

$$\hat{\mathbf{N}}_{A\theta}(t_k) = \begin{bmatrix} \hat{N}_{A\theta,1}(t_k) \\ \hat{N}_{A\theta,2}(t_k) \\ \vdots \\ \hat{N}_{A\theta,N_s}(t_k) \end{bmatrix} \quad (25)$$

$$\mathbf{C}(t_k) = \begin{bmatrix} C_1(t_k) \\ C_2(t_k) \\ \vdots \\ C_{N_s}(t_k) \end{bmatrix} \quad (26)$$

where $\mathbf{C}(t_k)$ is a vector containing the estimated concentrations of target molecules at the k^{th} time for all sensor locations. For a Markov system, the joint probability distribution can be expressed as

$$J_{MLE}(\mathbf{C}(t_k), k=0, \ldots, N-1) = \prod_{j=1}^{N_s}\prod_{k=1}^{N} \Pr(\hat{N}_{A\theta,j}(t_k) | \hat{N}_{A\theta,j}(t_{k-1}), C_j(t_{k-1})) \quad (27)$$

The binomial distribution (21), which was derived for an arbitrary starting state, can be used in the place of the conditional probability distributions appearing in the objective function (27) as

$$J_{MLE}(\mathbf{C}(t_k), k=0, \ldots, N-1) = \prod_{j=1}^{N_s}\prod_{k=1}^{N} \begin{pmatrix} B(\hat{N}_{A\theta,j}(t_{k-1}), \lambda^F(t_{k-1})) \\ * B(N_T - \hat{N}_{A\theta,j}(t_{k-1}), \lambda^E(t_{k-1})) \end{pmatrix} \quad (28)$$

Optimal estimates of the adsorption parameters $\mathbf{C}(t_k)$, k=0, …, N−1 are obtained by maximizing the objective function for the given measurement sequence $\hat{\mathbf{N}}_{A\theta}(t_k)$. Typically, a logarithm of the objective function J_{MLE} (28) is maximized instead to convert the multiplications into summations for the convenience of numerical operation:

$$\max_{\mathbf{C}(t_k),\, k=0,\ldots,N-1} \log J_{MLE} \quad (29)$$

The binomial distribution is in the exponential family of which logarithm for parameter set is concave [19].

For constant concentration, $\mathbf{C}(t_k)$ is equal to $\mathbf{C}$ for all time steps k=0, …, N−1. For time-varying concentration, the elements of $\mathbf{C}(t_k)$ may be correlated spatially and temporally according to some underlying governing equation (e.g., the diffusion equation) for the fluid phase that surrounds the carbon-nanotube-based sensor arrays.

2. Least Squares Estimation

The objective function in LSE is the sum of the squared errors between the measurement data $\hat{\mathbf{N}}_{A\theta}(t_k)$ and calculated data $\tilde{\mathbf{N}}_{A\theta}(t_k)$:

$$J_{LSE}(\mathbf{C}(t_k), k=0, \ldots, N-1) = \sum_{j=1}^{N_s}\sum_{k=1}^{N} (\hat{N}_{A\theta,j}(t_k) - \tilde{N}_{A\theta,j}(t_k))^2 \quad (30)$$

$\tilde{N}_{A\theta,j}(t_k)$ can be substituted by the expression in (16) for both constant and time-varying concentrations. Optimal estimates of the concentration sequence are obtained by minimizing the objective function

$$\min_{\mathbf{C}(t_k),\, k=0,\ldots,N-1} J_{LSE} \quad (31)$$

CASE STUDY: SINGLE SENSOR

1. Kinetic Monte Carlo Simulation

Since it is difficult to perform a fair and thorough comparison of the two estimation methods using an experimental setup, given the large stochastic variations, representative stochastic data sets were generated from the KMC simulations. Each KMC simulation run can be viewed as a particular realization of the stochastic system that is described by the CME. The adsorption/desorption process involves fairly simple molecular events and Zhang et al. [11] showed that experimental data for this system were well described by the KMC when the adsorption rate is much larger than the desorption rate.

For constant concentration, four different values of the concentration are evaluated. In the particular numerical study, the number of adsorbed molecules on the sensor is allowed to range from 0 to 10, so the number of possible discrete states is 11. The simulation time is 600 s. The starting state is assumed to be 0 (empty of molecules), which is assumed to be unknown to the estimator. It is also assumed that no two events can occur simultaneously. For generating both adsorption and desorption occurrences in the sample data, the k_A and k_D are assumed to be 1 and 0.01, respectively. The plots in Fig. 4 show three representative realizations of the time profile of the number of adsorbed molecules (chosen from the 10,000 kMC runs) for four different constant local concentrations. The

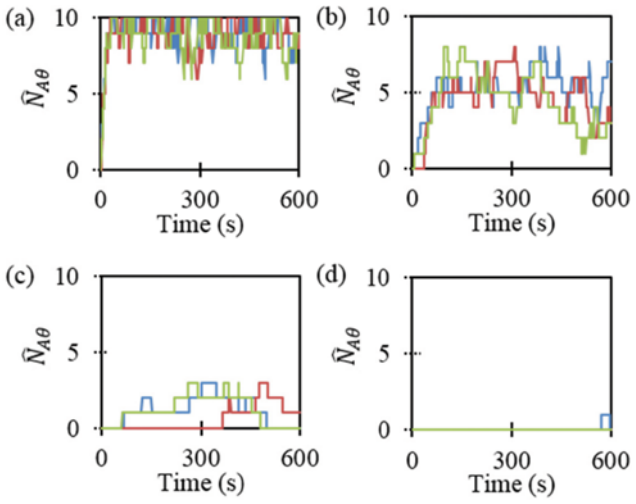

Fig. 4. Measurement data generated by running KMC simulations for a constant concentration of (a) 10^{-1}, (b) 10^{-2}, (c) 10^{-3}, and (d) 10^{-4} for k_A=1 and k_D=0.01.

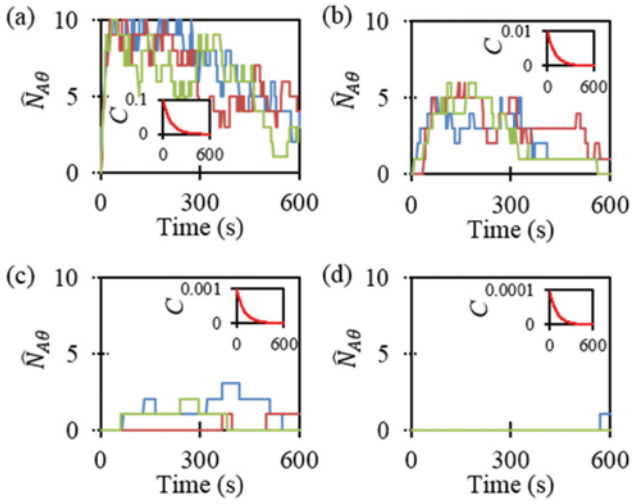

Fig. 5. Time plots of the adsorption data generated by running KMC simulations for a time-varying concentration profile, C(t), decreasing exponentially, starting at C_0 of (a) 10^{-1}, (b) 10^{-2}, (c) 10^{-3}, and (d) 10^{-4}, with the decay factor α=−0.005, k_A=1, and k_D=0.01.

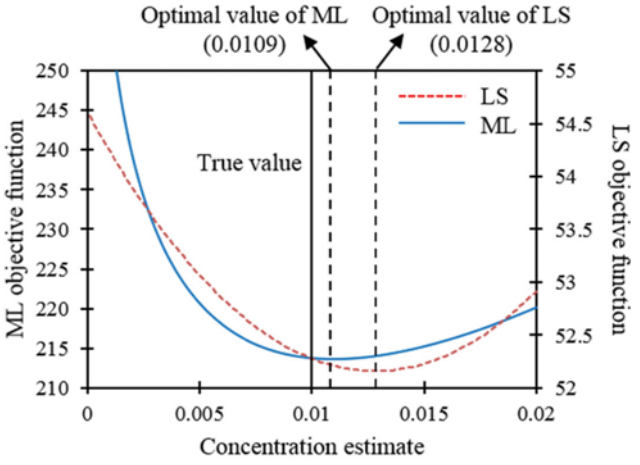

Fig. 6. Plot of the objective functions of MLE and LSE with respect to varying local concentration estimate.

adsorption data show distinct time profiles for the five different realizations even for the same local concentration, indicating significant stochastic characteristics in the system behavior. For C=10^{-4}, two of the three runs have adsorption events occurring rarely, due to the low adsorption rate (Fig. 4(d)).

In a real environment, the concentration of free target molecules surrounding a sensor is time varying. To assess the performance of the estimators in such a situation, it is assumed that the local concentration follows an exponential decay function with an initial value of C_0 and a decay factor of α:

$$C(t_k)=C_0e^{-\alpha t_k} \tag{32}$$

With such time-varying C(t), measurement data are generated by running the KMC simulation of the CME (see Fig. 5). Similarly, as before (as seen from Fig. 4), significant stochastic variations are observed.

2. Estimation Results for Constant Concentration

Data from KMC simulation runs were used to test and compare the performance of the two estimation methods. One of MATLAB's constrained optimization programs, sequential quadratic programming (SQP) in fmincon, was used to solve the optimizations in both MLE and LSE with a feasible parameter range of:

$$10^{-6}\le C_{k,j}\le 10^{6},\ k=1,\ \ldots,\ N,\ j=1,\ \ldots,\ N_S \tag{33}$$

The initial guess was set as 10^{-5} in all cases. The analytical solution (16) of the continuum Eq. (12) was used for both the constant and time-varying concentrations.

First, the behavior of the objective functions of the MLE (28) and LSE (30) with respect to varying local concentration estimate is investigated using data generated from one run (600 samples) with constant C of 10^{-2} (Fig. 6). The shape of the ML objective function is a typical negative log-likelihood curve that is steeper and more compressed in scale than that of the LS objective function. For this particular case, the optimal value of ML is observed to be closer to the true value than that of LS, which happens more frequently in repeated runs.

In Table 1, the estimated values of the local concentration (given at the end of a run) averaged over the 10,000 runs (600-sample dataset per one run) except for the cases of failures and their relative root-mean-square errors (RMSEs) in percentage are compared for four different values of constant concentrations. The %RMSE in the table is defined by

$$\%\text{RMSE}=100\sqrt{\sum_{j=1}^{N_S}\sum_{k=1}^{N}\left(\frac{C_{true}-\hat{C}_{k,j}}{C_{true}}\right)^2\Big/(N_SN)} \tag{34}$$

Table 1. Estimation results for four constant concentrations of 10^{-1}, 10^{-2}, 10^{-3}, and 10^{-4} (averaged results from 10,000 runs with 600 samples per run)

True C (mole)	Methods	Averaged estimate of C (mole)	%RMSE of the estimate (%)	Number of estimation failure (trials)
10^{-1}	MLE	1.016×10^{-1}	13.7	0
	LSE	1.034×10^{-1}	18.5	0
10^{-2}	MLE	1.015×10^{-2}	18.2	0
	LSE	1.042×10^{-2}	24.2	0
10^{-3}	MLE	1.019×10^{-3}	43.6	26
	LSE	1.052×10^{-3}	59.7	26
10^{-4}	MLE	2.257×10^{-4}	196.9	5507
	LSE	2.314×10^{-4}	265.3	5507

In all cases, the average estimated values for MLE are closer to the true values than for LSE. In addition, the %RMSE of the estimates for MLE are significantly smaller than for LSE in all cases. For C=10^{-4}, the %RMSE for both methods show very high values, and more than half of the 10,000 estimation trials have failed to give a reliable solution. This reduced estimation performance is inherent in the experimental data for this very low concentration, as most of the datasets contain rare or even no adsorption events (see Fig. 4(d)). At this low concentration region, an accurate estimation may be impossible regardless of the method used.

3. Detectable Range Analysis

An analysis of detectable concentration range for the SWNT-based sensor is not available in previous mathematical analyses published in the literature. Instead, the concentration range where experimental adsorption time profiles obtained has been roughly mentioned for different sensor designs and target molecules individually. For using the developed sensors in real applications such as in control systems, the lower and upper limits of the detectable concentration range for given sensor and target molecules should be clearly determined and provided as a key sensor property. Also, the lower and upper limit analysis could provide feedback about sensor design modification or improvement for use in a desired detectable range. Simulation-based analysis with sufficient KMC runs is expected to provide the limits.

For a single sensor, the low analyte concentration range from C=10^{-4} to C=10^{-3} is explored more densely to determine the lower limit of detection. Fig. 7 shows a histogram of estimates from 10,000 trials (600 s run per one trial) of the MLE for each true concentration with. At a concentration less than 3×10^{-4}, more than 16% of the estimation trials failed as indicated by a separated peak at the left in Fig. 7. For a concentration greater than 4×10^{-4}, more than 90% of the estimation trials give reliable solutions. To estimate the analyte concentration at the lower value range with higher confidence, the sensor should be designed to have a larger k_A value, which is associated with a higher sensitivity for the target molecules.

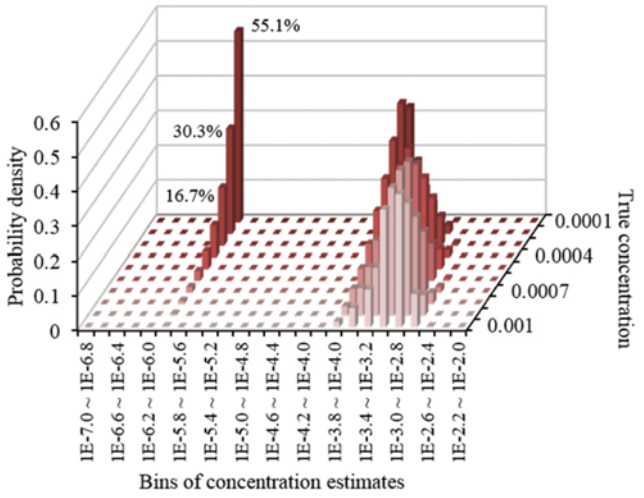

Fig. 7. Histogram of the concentration estimates from 10,000 trials of MLE for concentrations ranging from C=10^{-4} to C=10^{-3} ("E-d" in the horizontal axis means 10^{-d}).

The upper limit concentration can be seen by comparing the averaged estimation value in Table 2. For concentrations higher than 1, the estimation trial always gave a solution without failure, but the averaged estimates cannot break the bound of around 2000 mole for MLE and 200 mole for LSE. Especially, a concentration higher than 1000 is so high that saturation of the possible adsorption sites occurs too quickly at early stage and after that rare desorption occurs as shown in the second column of Table 2. Opposite to the design needed to extend the lower limit, the sensor design should have smaller k_A value for estimating higher values of the analyte concentration.

4. Effects of Parameter Mismatch

Throughout this paper, the MLE and LSE for estimating the local concentration near the sensor assume that the true values of the rate constants, k_A and k_D are known exactly. However, in reality, a mismatch in these parameters can exist between the stochastic ad-

Table 2. Estimation results for constant concentrations higher than (averaged results from 10,000 runs with 600 samples per run)

True C (mole)	Averaged # of adsorption/ # of desorption in one run	Methods	Averaged estimate of C (mole)	%RMSE of the estimate (%)
1	45.17/35.27	MLE	0.964	7.9
		LSE	0.927	12.8
10	15.89/5.90	MLE	11.47	47.1
		LSE	11.47	47.3
10^2	10.06/0.06	MLE	133.5	81.7
		LSE	200.0	100.0
10^3	10.01/0.01	MLE	1887.21	99.7
		LSE	205.02	79.5
10^4	10.00/0.00	MLE	2546.8	74.6
		LSE	204.9	98.0
10^5	10.00/0.00	MLE	2119.1	97.9
		LSE	204.9	99.8
10^6	10.00/0.00	MLE	2119.5	99.8
		LSE	204.9	100.0

sorption model and the actual sensing system. To see the effect of potential mismatches in them, we applied ±10% and ±20% variations to the assumed k_A and k_D values in the model equations of (14) and (21)-(23) for LSE and MLE, respectively. The sample data used are the data generated by the KMC simulations in the subsection 2. Based on the detection range analysis in the subsection 3, the concentrations of $C=10^{-1}$ and $C=10^{-2}$, which showed no failure in the estimation, are considered in this analysis.

Table 3 shows the averaged estimation results for 10,000 trials with the mismatch of k_A. For the cases of −10% and −20% variations, the estimates from MLE are closer to the true value than LSE. On the other hand, for the cases of +10% and +20% variations, the opposite results are obtained. As defined in Eq. (6), the adsorption rate constant and the concentration to be estimated are closely interconnected as a pair with multiplication. For this reason, when we have a positive variation in k_A, the estimated concentration is decreased and vice versa. The larger positive biases seen in the esti-

Table 3. Estimation results for constant concentrations of 10^{-1} and 10^{-2} with mismatch in k_A (averaged results from 10,000 runs with 600 samples per run)

Mismatch	True C (mole)	Methods	Averaged estimate of C (mole)	%RMSE of the estimate (%)
−10% of k_A	10^{-1}	MLE	1.129×10^{-1}	19.9
		LSE	1.149×10^{-1}	25.1
	10^{-2}	MLE	1.128×10^{-2}	23.8
		LSE	1.158×10^{-2}	30.8
+10% of k_A	10^{-1}	MLE	9.239×10^{-2}	14.6
		LSE	9.400×10^{-2}	17.6
	10^{-2}	MLE	9.225×10^{-3}	18.2
		LSE	9.471×10^{-3}	22.3
−20% of k_A	10^{-1}	MLE	1.270×10^{-1}	32.0
		LSE	1.292×10^{-1}	37.1
	10^{-2}	MLE	1.268×10^{-2}	35.1
		LSE	1.302×10^{-2}	42.4
+20% of k_A	10^{-1}	MLE	8.469×10^{-2}	19.1
		LSE	8.617×10^{-2}	20.5
	10^{-2}	MLE	8.456×10^{-3}	21.6
		LSE	8.682×10^{-3}	23.8

Table 4. Estimation results for constant concentrations of 10^{-1} and 10^{-2} with mismatch in k_D (averaged results from 10,000 runs with 600 samples per run)

Mismatch	True C (mole)	Methods	Averaged estimate of C (mole)	%RMSE of the estimate (%)
−10% of k_D	10^{-1}	MLE	1.004×10^{-1}	13.4
		LSE	9.995×10^{-2}	17.8
	10^{-2}	MLE	1.010×10^{-2}	18.0
		LSE	9.727×10^{-3}	22.5
+10% of k_D	10^{-1}	MLE	1.029×10^{-1}	14.2
		LSE	1.067×10^{-1}	19.8
	10^{-2}	MLE	1.020×10^{-2}	18.4
		LSE	1.111×10^{-2}	27.6
−20% of k_D	10^{-1}	MLE	9.921×10^{-2}	13.2
		LSE	9.688×10^{-2}	17.7
	10^{-2}	MLE	1.005×10^{-2}	17.8
		LSE	9.037×10^{-3}	22.9
+20% of k_D	10^{-1}	MLE	1.042×10^{-1}	14.7
		LSE	1.100×10^{-1}	21.5
	10^{-2}	MLE	1.025×10^{-2}	18.6
		LSE	1.180×10^{-2}	32.3

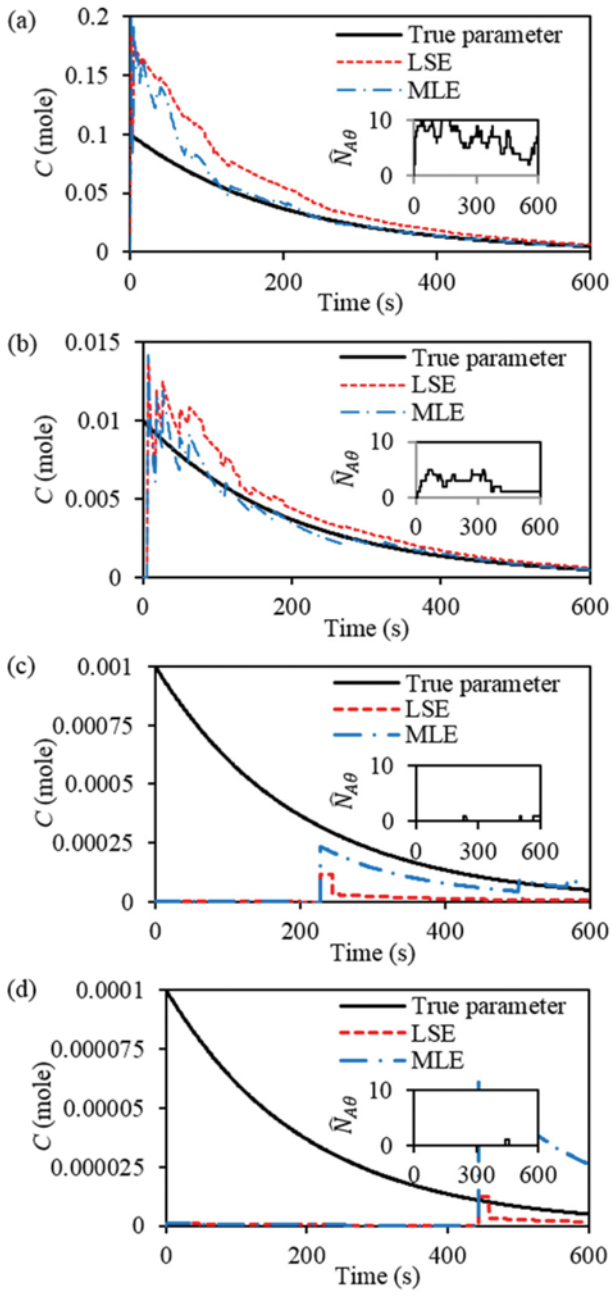

Fig. 8. Time plots of the measurements for the number of adsorbed molecules (inset) and the LSE and MLE estimates for time-varying C(t) exponentially decreasing from an initial value of (a) 10^{-1}, (b) 10^{-2}, (c) 10^{-3}, and (d) 10^{-4}.

mates from LSE, as shown in Table 1, are further increased the error in the estimates caused by the negative variation in the parameter. On the other hand, the very bias of LSE actually ends up compensating for the decrease in the estimates caused by the positive variations.

In case of the mismatch of k_D, the average estimates from MLE are closer to the true value than LSE in all cases (Table 4). The effect of k_D on the concentration is not as significant as k_A. In both methods, the estimates tend to increase for the positive variation, and decrease for the negative variation, and the amounts of increase and decrease in LSE are larger than those in MLE.

Above all, the RMSEs of MLE for both mismatches in k_A and k_D always show smaller values than LSE, which indicates that the estimates from MLE are more narrowly distributed around the true value than LSE. In conclusion, despite the mismatch, the performance advantage of MLE over LSE is still maintained.

5. Estimation Results for Time-varying Concentration

For time-varying concentration, the concentration was modeled as following the exponentially decaying function (32). The performance of the two methods can be compared by observing how well the concentration estimates track the true concentration profile throughout the run time. Plots showing the estimation performances for exemplary KMC simulation runs are in Fig. 8.

The MLE estimates follow the true concentration more closely than the LSE counterpart for concentration C starting from 10^{-1} and 10^{-2} (see Fig. 8(a), (b)). For concentration C starting from 10^{-3} and 10^{-4}, neither estimation method can reasonably estimate the concentration until an adsorption event actually occurs (see Fig. 8(c), (d), including insets), which is expected since there is very little information in the data up to that time. The lack of detection of an adsorption event for a certain period of time limits the estimates for the concentration from being much larger than zero (Fig. 8(c), (d)). As time increases, the true concentration value eventually becomes simply too small to be tracked closely, which is most evident in the last simulation (Fig. 8(d)). Without a sufficient number of adsorption events occurring, accurate estimation is not possible regardless of the method employed.

These results illustrate an important characteristic of single molecule detection: The estimation problem becomes very asymmetric for low adsorption rates. Since the rates are proportional to the local fluid concentration, these results also indicate that no estimation method can be effective at fluid concentrations below the detection limit for given adsorption parameter. For local fluid concentrations that are high enough to enable sufficient adsorption/desorption events to occur, the MLE method based on the CME produces more accurate results than the standard approach of applying LSE to the continuum model, as can be seen from Table 5 and Fig. 8(a), (b).

Table 5. Estimation results for a time-varying true concentration $C(t_k)=C_0e^{-\alpha t_k}$ (averaged results from 10,000 runs with 600 samples per run)

Initial true C_0 (mole)	Methods	RMSE of the estimate
10^{-1}	MLE	1.676×10^{-2}
	LSE	2.710×10^{-2}
10^{-2}	MLE	2.973×10^{-3}
	LSE	4.287×10^{-3}

SENSOR ARRAY

In Section 5.4, the estimation was formulated for a single isolated sensor using simple concentration dynamics such as an exponential decay. In reality, multiple sensors are placed in an array structure to measure two-dimensional concentration profiles, of which spatial and temporal patterns are governed by underlying physical phenomena such as diffusion (see Fig. 2).

This section expands the previous section's results to a 2D sensor array in which a trace of target molecules are injected in the center of the array (Fig. 9(a)). The injected molecules then diffuse from the center towards the edges and out of the system as time goes on (Fig. 9(b)). Depending on the value of the diffusion coefficient, the rate of reaching zero concentration can be slowed down or accelerated.

The measurement values are assumed to be obtained at every sampling time from the sensors, which are distributed in a 2D array structure of uniform spacing along the x and y directions. The local concentration of target molecules at each sensor is assumed to follow the diffusion phenomenon described by

$$\frac{\partial C(x, y, t)}{\partial t} = D\nabla^2 C(x, y, t) \tag{35}$$

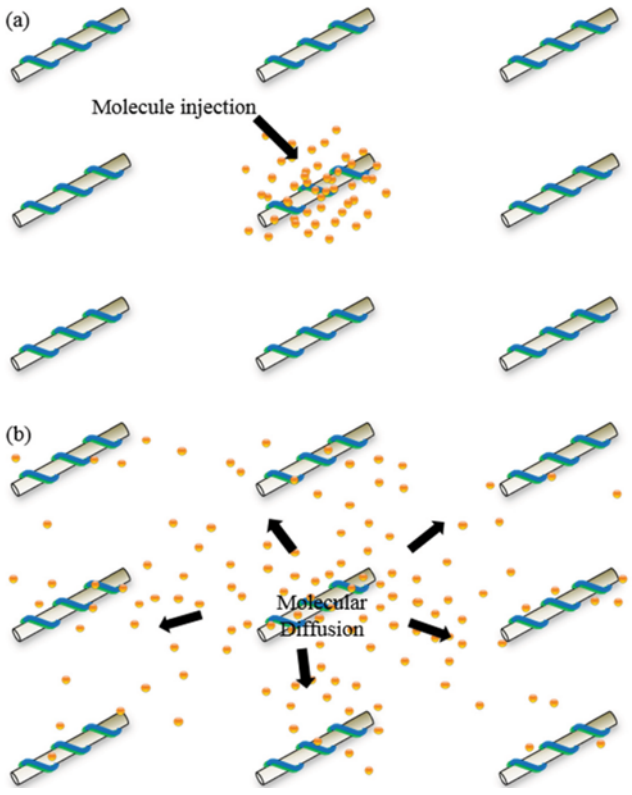

Fig. 9. Mass transfer phenomena of target molecules on a 3×3 sensor array system, (a) injection of trace molecules at the center and (b) diffusion across the sensor array.

where C(x, y, t) is the concentration of a target molecule at position (x, y) and D is the diffusion coefficient, which is assumed to be known. This description is adequate for diffusion in which the local solution concentration is high enough that depletion from the liquid phase due to adsorption onto sensors is negligible. For very low concentration of target molecules, the transport would be better described using stochastic models like Brownian motion or random walk. Modeling of such molecular transport is beyond the scope of this work, in which the interest is in processing the information from multiple sensors with the MLE and LSE methods.

For a uniform mesh of size (Δx, Δy) and a constant discretization time $\Delta t=t_{k+1}-t_k$, the partial differential Eq. (35) can be approximated by a set of discrete-time equations by using the finite difference method [20]:

$$\frac{C_{i,j}^{k+1}-C_{i,j}^{k}}{\Delta t}=D\left(\frac{C_{i+1,j}^{k}-2C_{i,j}^{k}+C_{i-1,j}^{k}}{(\Delta x)^2}+\frac{C_{i,j+1}^{k}-2C_{i,j}^{k}+C_{i,j-1}^{k}}{(\Delta y)^2}\right) \tag{36}$$

$$C(x_i, y_j, t_k)\equiv C_{i,j}^{k};\ i=1, \ldots, n_x;\ j=1, \ldots, n_y;\ k=0, \ldots, n_T \tag{37}$$

By sequentially numbering the nodes at mesh points, the equations can be written into the standard discrete-time state-space system structure:

$$\mathbf{x}_{k+1}=\mathbf{A}\mathbf{x}_k \tag{38}$$

$$\mathbf{x}_k=[C_{1,1}^{k}\ C_{2,1}^{k}\ \cdots\ C_{i,j}^{k}\ C_{i+1,j}^{k}\ \cdots\ C_{n_x-1,n_y}^{k}\ C_{n_x,n_y}]^T \tag{39}$$

$$\mathbf{A}=\begin{bmatrix} \mathbf{A}_1 & \mathbf{A}_2 & \mathbf{0} & \cdots & \cdots & \mathbf{0} \\ \mathbf{A}_2 & \mathbf{A}_1 & \mathbf{A}_2 & \ddots & \ddots & \vdots \\ \mathbf{0} & \mathbf{A}_2 & \ddots & \ddots & \ddots & \vdots \\ \vdots & \ddots & \ddots & \ddots & \mathbf{A}_2 & \mathbf{0} \\ \vdots & \ddots & \ddots & \mathbf{A}_2 & \mathbf{A}_1 & \mathbf{A}_2 \\ \mathbf{0} & \cdots & \cdots & \mathbf{0} & \mathbf{A}_2 & \mathbf{A}_1 \end{bmatrix} \tag{40}$$

$$\mathbf{A}_1=\begin{bmatrix} 1-2s_x-2s_y & s_x & 0 & \cdots & \cdots & 0 \\ s_x & 1-2s_x-2s_y & s_x & \ddots & \ddots & \vdots \\ 0 & s_x & \ddots & \ddots & \ddots & \vdots \\ \vdots & \ddots & \ddots & \ddots & \ddots & s_x \\ \vdots & \ddots & \ddots & \ddots & s_x & 0 \\ 0 & \cdots & \cdots & s_x & 1-2s_x-2s_y & s_x \\ & & & 0 & s_x & 1-2s_x-2s_y \end{bmatrix} \tag{41}$$

$$\mathbf{A}_2=\begin{bmatrix} s_y & 0 & \cdots & 0 \\ 0 & s_y & \cdots & 0 \\ \vdots & \vdots & \ddots & \vdots \\ 0 & 0 & \cdots & s_y \end{bmatrix} \tag{42}$$

$$s_x=D\frac{\Delta t}{(\Delta x)^2} \tag{43}$$

$$s_y=D\frac{\Delta t}{(\Delta y)^2} \tag{44}$$

where each **0** refers to the appropriately dimensioned null matrix whose entries are all zeros. The $n_x n_y \times n_x n_y$ system matrix **A** has a symmetric structure interconnecting the nearby nodes. If sensors are placed on all the nodes, Eq. (38) can be directly related to the local concentration $\mathbf{C}(t_k)$ near the sensor.

Then, the spatiotemporal variations of the adsorption parameter can be expressed as

$$\mathbf{C}(t_{k+1})=\mathbf{A}\mathbf{C}(t_k), \tag{45}$$

which can be used as constraints in both MLE (28) and LSE (30) formulations.

This numerical study considers a 3×3 sensor array with uniform spacing of 0.5 between the sensors placed along the x and y directions. From the nine individual sensors, adsorption data reflecting the local concentrations can be obtained every 1 second. By setting $k_A=1$, $k_D=0.01$, $D=0.005$, and the initial condition

$$\mathbf{C}_0=[0\ 0\ 0\ 0\ 0.1\ 0\ 0\ 0\ 0], \tag{46}$$

which indicates a trace injection at (0.5,0.5) at t=0, typical KMC simulation data for the nine locations can be obtained (Fig. 10). As this system has adsorption rates similar to or smaller than the desorption rate in magnitude, frequent adsorption and desorption events can be observed in the data from all locations.

Due to the symmetric nature of the diffusion system, the sample data for the pairs [(0,0), (0,1), (1,0), (1,1)] and [(0,0.5), (0.5,0), (0.5,1), (1,0.5)] were all generated with the same concentration time profiles, respectively, in the KMC simulation (Fig. 11). However, the KMC realizations for the pairs showed very different adsorption time profiles, indicating the significant stochastic characteristics of the system. In addition, locations far from the center

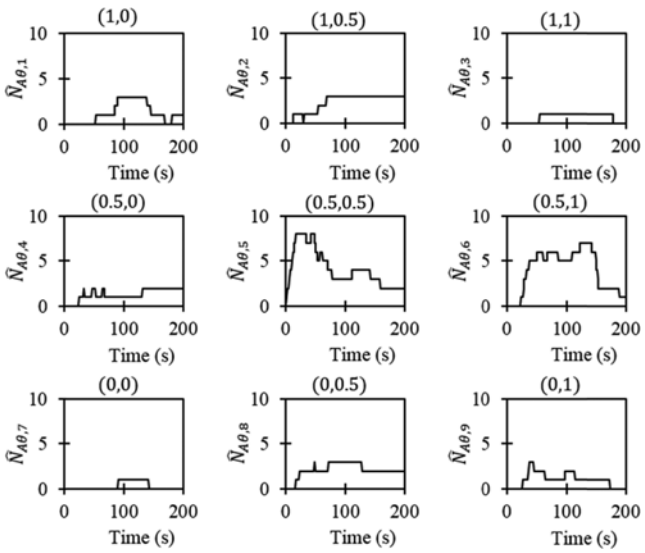

Fig. 10. Sample data generated by the KMC simulation for different sensor locations in a 3×3 sensor array system with k_A= 1, and k_D=0.01, and D=0.005.

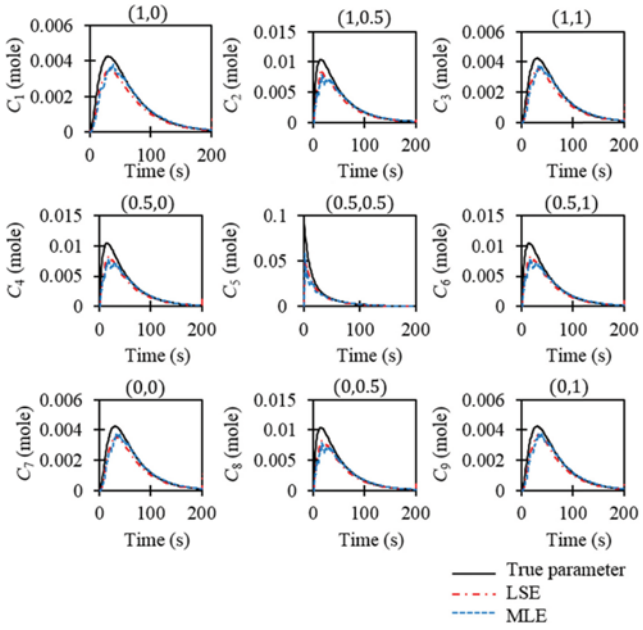

Fig. 11. True vs. estimated parameters for the 9 locations in the 3×3 sensor array system with k_A=1, and k_D=0.01, and D=0.005.

(e.g., [(0,0), (0,1), (1,0), (1,1)]) showed no adsorption events for a significant initial period of time. Results in Section 5.4 showed that accurate estimation using a single local sensor is impossible regardless of method.

Fig. 11 and Table 6 show the estimation results of the proposed MLE and LSE using the multiple sensor data in Fig. 10. While there is some error in short time, the MLE estimates track the true concentration dynamics quite well for all the locations with less bias than for LSE. In addition, at the locations [(0,0), (0,1), (1,0), (1,1)], accurate estimation starts even before an adsorption event occurs. The reason is that the diffusion Eqs. (45) correlate the concentrations for the entire spatial domain, and therefore good estimation at one sensor location can have an ameliorating effect at other sensor locations.

Table 6. Estimation results for the concentrations $C_{k+1}=AC_k$ at various locations (averaged results from 1,000 runs with 200 samples per run)

Sensor location	Methods	RMSE of estimates
(1,0)	MLE	4.428×10^{-3}
	LSE	4.490×10^{-3}
(1,0.5)	MLE	1.148×10^{-2}
	LSE	1.184×10^{-2}
(1,1)	MLE	4.020×10^{-3}
	LSE	4.554×10^{-3}
(0.5,0)	MLE	1.067×10^{-2}
	LSE	1.200×10^{-2}
(0.5,0.5)	MLE	2.493×10^{-2}
	LSE	2.547×10^{-2}
(0.5,1)	MLE	1.131×10^{-2}
	LSE	1.210×10^{-2}
(0,0)	MLE	3.924×10^{-3}
	LSE	4.065×10^{-3}
(0,0.5)	MLE	1.175×10^{-2}
	LSE	1.253×10^{-2}
(0,1)	MLE	4.363×10^{-3}
	LSE	4.548×10^{-3}
All	MLE	1.156×10^{-2}
	LSE	1.209×10^{-2}

As an additional case study for the 3×3 sensor array system, signals with random tracer injections on all sensors at every 200 seconds are tried to check the tracking performance of MLE. With k_A=1, k_D=0.01 and D=0.005, a total of 100 datasets (nine time-profiles in one dataset) are generated from the KMC simulation, for example, in the left side of Fig. 12. The estimation was performed with the assumption that the injection timing is known. At every 200 seconds, the estimation is re-initialized for the unknown intermediate injections. The initial state on each sensor is not zero, which indicates some adsorption sites are occupied. From the estimation results in the right side of Fig. 12, we can confirm that MLE gives a better tracking performance than LSE. The calculated RMSE of MLE (0.0127) is smaller than that of LSE (0.0130).

This study establishes the possibility of using the proposed MLE method to estimate a spatiotemporal concentration profile with a sensor array placed on a two-dimensional field. Importantly, the proposed MLE method, when used with physical constraints correlating the spatiotemporal data from multiple sensors, can enjoy extended detection ranges to include those regions with very low concentrations of molecules.

CONCLUSIONS

For an inherently stochastic adsorption process, maximum likelihood estimation based on an analytical solution of the chemical master equation was shown to provide more accurate local concentration estimates (with less bias and variance) than least squares estimation. This conclusion is valid for concentrations resulting in sufficient adsorption events so that the sensor produces enough information for the estimation to become feasible. For sensor arrays where not only adsorption events but also desorption events occurred frequently, the proposed MLE method showed a good tracking performance even for regions of very low concentration.

The results can be viewed as a first step towards a complete methodology for state/parameter estimation of a distributed parameter system integrated with a nano-sensor array system. Our eventual goal is to build an optimal recursive state estimator for 2D concentration fields of target molecules present in small quantity, and use the estimated concentration fields in a control system designed to achieve a specified 2D spatial control objective. Such an estimator can be useful in many emerging applications including in the biomedical field. For example, the real-time estimates of concentration profile could be fed into an optimal control system that injects special molecules into the process to achieve specific temporal and spatial concentration patterns, which induce a desired stem cell differentiation [21]. Many challenges remain, including the modeling of molecular transport when target molecules are present in trace

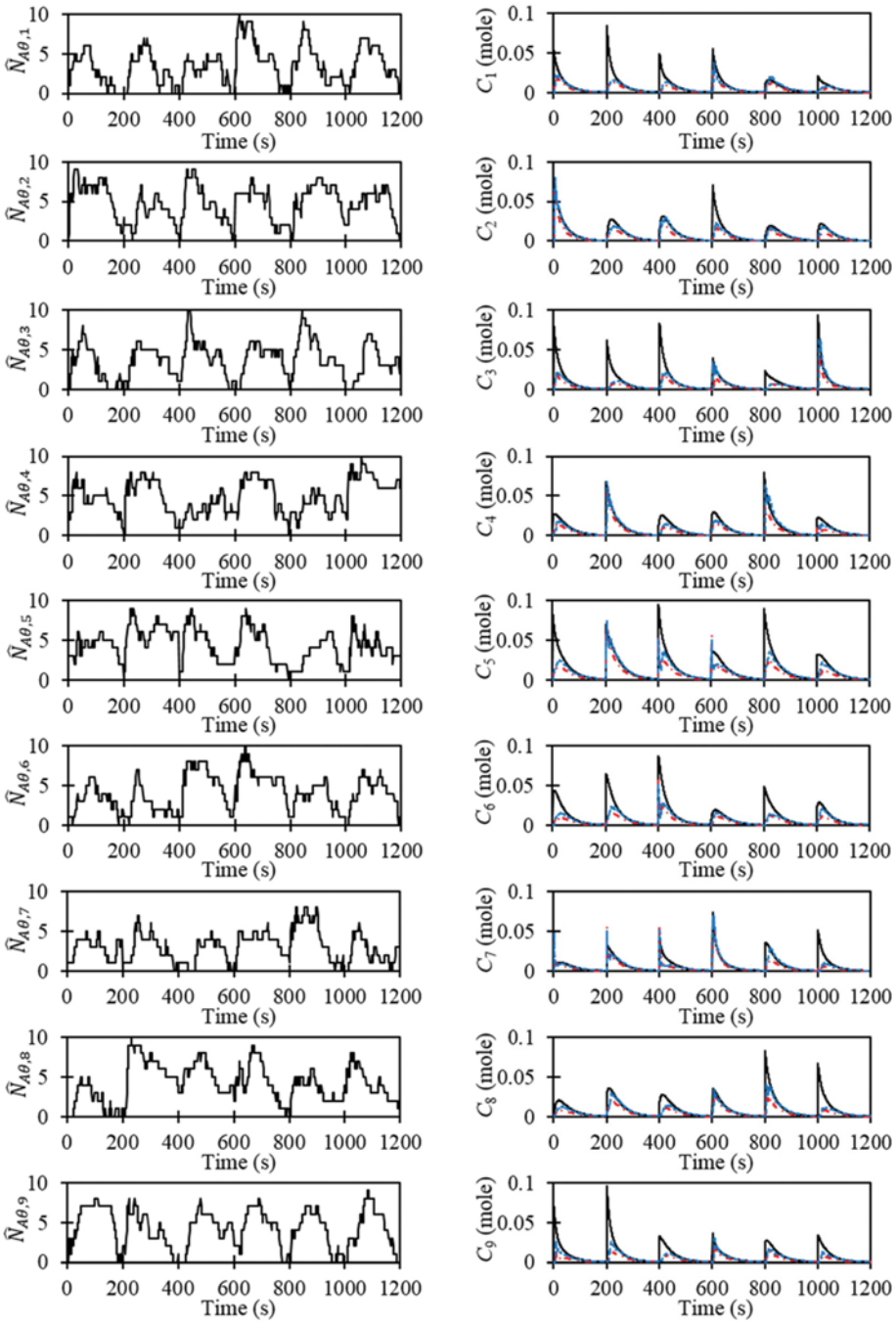

Fig. 12. Sample data for random injections made every 200 seconds on the 3×3 sensors and the corresponding LES/MSE estimated concentration values with k_A=1, and k_D=0.01, D=0.005.

quantities.

ACKNOWLEDGEMENT

This work was supported by the Advanced Biomass R&D Center (ABC) of Global Frontier Project funded by the Ministry of Science, ICT and Future Planning (ABC-0031354).

REFERENCES

1. H.-N. Umh, H. H. Shin, J. Yi and Y. Kim, *Korean J. Chem. Eng.*, **32**, 299 (2015).
2. S. R. Ahmed, K. Koh, E. Y. Park and J. Lee, *Korean J. Chem. Eng.*, **30**, 1825 (2013).
3. S. Saito and A. Zettl, *Carbon Nanotubes: Quantum Cylinders of Graphene*, Elsevier (2008).
4. A. A. Boghossian, J. Zhang, P. W. Barone, N. F. Reuel, J. H. Kim, D. A. Heller, J. H. Ahn, A. J. Hilmer, A. Rwei and J. R. Arkalgud, *ChemSusChem*, **4**, 848 (2011).
5. L. Cognet, D. A. Tsyboulski, J.-D. R. Rocha, C. D. Doyle, J. M. Tour and R. B. Weisman, *Science*, **316**, 1465 (2007).

6. P. W. Barone, S. Baik, D. A. Heller and M. S. Strano, *Nature Mater.*, **4**, 86 (2005).
7. D. A. Heller, E. S. Jeng, T.-K. Yeung, B. M. Martinez, A. E. Moll, J. B. Gastala and M. S. Strano, *Science*, **311**, 508 (2006).
8. J. H. Kim, J. H. Ahn, P. W. Barone, H. Jin, J. Zhang, D. A. Heller and M. S. Strano, *Angew. Chem.*, **122**, 1498 (2010).
9. H. Jin, D. A. Heller, M. Kalbacova, J.-H. Kim, J. Zhang, A. A. Boghossian, N. Maheshri and M. S. Strano, *Nature Nanotech.*, **5**, 302 (2010).
10. H. Jin, D. A. Heller, J.-H. Kim and M. S. Strano, *Nano Lett.*, **8**, 4299 (2008).
11. J. Zhang, A. A. Boghossian, P. W. Barone, A. Rwei, J.-H. Kim, D. Lin, D. A. Heller, A. J. Hilmer, N. Nair and N. F. Reuel, *J. Am. Chem. Soc.*, **133**, 567 (2010).
12. J.-H. Kim, D. A. Heller, H. Jin, P. W. Barone, C. Song, J. Zhang, L. J. Trudel, G. N. Wogan, S. R. Tannenbaum and M. S. Strano, *Nature Chem.*, **1**, 473 (2009).
13. K. A. Fichthorn and W. H. Weinberg, *J. Chem. Phys.*, **95**, 1090 (1991).
14. T. Jahnke and W. Huisinga, *J. Math. Biol.*, **54**, 1 (2007).
15. A. A. Boghossian, J. Zhang, F. T. Le Floch-Yin, Z. W. Ulissi, P. Bojo, J.-H. Han, J.-H. Kim, J. R. Arkalgud, N. F. Reuel and R. D. Braatz, *J. Chem. Phys.*, **135**, 084124 (2011).
16. Z. W. Ulissi, J. Zhang, A. A. Boghossian, N. F. Reuel, S. F. Shimizu, R. D. Braatz and M. S. Strano, *J. Phys. Chem. Lett.*, **2**, 1690 (2011).
17. Z. W. Ulissi, M. S. Strano and R. D. Braatz, *Comput. Chem. Eng.*, **51**, 149 (2013).
18. M. Kishida and R. D. Braatz, *Optimal spatial field control of distributed parameter systems*, American Control Conference 2009, IEEE, 32 (2009).
19. E. L. Lehmann and J. P. Romano, *Testing statistical hypotheses*, Springer (2006).
20. H. Jang, J. H. Lee, R. D. Braatzf and K.-K. K. Kim, *Comput. Chem. Eng.*, **63**, 159 (2013).
21. M. Kishida, D. W. Pack and R. D. Braatz, *State-constrained optimal spatial field control for controlled release in tissue engineering*, American Control Conference 2010, IEEE, 4361 (2010).